Multi-peak accumulation and coarse modes observed from AERONET retrieved aerosol volume size distribution in Beijing

Ying Zhang, Zhengqiang Li, Yuhuan Zhang, Yu Chen, Juan Cuesta, Yan Ma

Meteorology and Atmospheric Physics

Multi-peak accumulation and coarse modes observed from AERONET retrieved aerosol volume size distribution in Beijing

--Manuscript Draft--

Manuscript Number:	MAAP-D-15-00155R2
Full Title:	Multi-peak accumulation and coarse modes observed from AERONET retrieved aerosol volume size distribution in Beijing
Article Type:	Original Paper
Corresponding Author:	Zhengqiang Li CHINA
Corresponding Author Secondary Information:	
Corresponding Author's Institution:	
Corresponding Author's Secondary Institution:	
First Author:	Ying Zhang
First Author Secondary Information:	
Order of Authors:	Ying Zhang
	Zhengqiang Li
	Yuhuan Zhang
	Yu Chen
	Juan Cuesta
	Yan Ma
Order of Authors Secondary Information:	

Funding Information:		
	National Natural Science Foundation of China (41222007)	Zhengqiang Li
	Chinese Academy of Sciences (KZZD-EW-TZ-18)	Zhengqiang Li
	Chinese Academy of Sciences (XDA05100202)	Zhengqiang Li
	Chinese Major Project of High Resolution Earth Observation System (30-Y20A39-9003-15/17)	Zhengqiang Li

Abstract: We present characteristic peaks of atmospheric columnar aerosol volume size distribution retrieved from the AErosol RObotic NETwork (AERONET) ground-based Sun-sky radiometer observation, and their correlations with aerosol optical properties and meteorological conditions in Beijing over 2013. The results show that the aerosol volume particle size distribution (VPSD) can be decomposed into up to four characteristic peaks, located in accumulation and coarse modes, respectively. The mean center radii of extra peaks in accumulation and coarse modes locate around 0.28(±0.09)-0.38(±0.11) and 1.25(±0.56)-1.47(±0.30) μm, respectively. The multi-peak size distributions are found in different aerosol loading conditions, with the mean aerosol optical depth (440 nm) of 0.58, 0.49, 1.18 and 1.04 for 2-, 3- I/II and 4-peak VPSD types, while the correspondingly mean relative humidity values are 58, 54, 72 and 67%, respectively. The results also show the significant increase (from 0.25 to 0.40 μm) of the mean extra peak median radius in the accumulation mode for the 3-peak-II cases, which agrees with aerosol hygroscopic growth related to relative humidity and/or cloud or fog processing.

COMMENTS TO THE AUTHOR:
Reviewer #2: MAP manuscript: Multi-peak accumulation and coarse modes observed from AERONET retrieved aerosol volume size distribution in Beijing

1. Abstract: line 46 - please add to the end of this sentence: "and/or cloud or fog processing.'

We have added "and/or cloud or fog processing" to the end of this sentence.

2. Line 158: Replace 'breaking down' with 'separation'

We have corrected according to the Reviewer's comments.

3. Line 239: The Klein and Daba (2014) reference is not pertinent here since this paper mainly focuses on fog droplet size and liquid water content of the fog droplets, not the residual aerosol that remains after fog evaporation. I suggest replacing this with Li et al. (2014)

Thanks for reviewer's comment. We have corrected according to the Reviewer's comments.

4. Line 251 : Please add: "and/or cloud or fog processing.'

We have added "and/or cloud or fog processing" according to the Reviewer's comments.

Multi-peak accumulation and coarse modes observed from AERONET retrieved aerosol volume size distribution in Beijing

Ying Zhang[1], Zhengqiang Li[1*], Yuhuan Zhang [2], Yu Chen[3], Juan Cuesta[4], Yan Ma[1]

1. State Environmental Protection Key Laboratory of Satellite Remote Sensing, Institute of Remote Sensing and Digital Earth, Chinese Academy of Sciences, Beijing 100101, China
2. Satellite Environment Center, Ministry of Environmental Protection of China, Beijing, 100094, China
3. Public Meteorological Service Center, China Meteorological Administration, Beijing 100081, China
4. Laboratoire Inter-Universitaire des Systèmes Atmosphériques, Université Paris Est Créteil, Créteil Cedex 94010, France

***Corresponding author address:**

Prof. Zhengqiang Li

Institute of Remote Sensing and Digital Earth, Chinese Academy of Sciences

Beijing 100101, China

E-mail: lizq@radi.ac.cn

Tel: +86 10 6485 7437 / Fax: +86 10 6480 6225

Highlights

- The 3-peak and 4-peak aerosol volume size distributions observed in Beijing.
- Characteristics of extra peaks in accumulation and coarse modes respectively.
- Statistics on multi-peak cases versus meteorological conditions.

Abstract

We present characteristic peaks of atmospheric columnar aerosol volume size distribution retrieved from the AErosol RObotic NETwork (AERONET) ground-based Sun-sky radiometer observation, and their correlations with aerosol optical properties and meteorological conditions in Beijing over 2013. The results show that the aerosol volume particle size distribution (VPSD) can be decomposed into up to four characteristic peaks, located in accumulation and coarse modes, respectively. The mean center radii of extra peaks in accumulation and coarse modes locate around 0.28(±0.09)-0.38(±0.11) and 1.25(±0.56)-1.47(±0.30) μm, respectively. The multi-peak size distributions are found in different aerosol loading conditions, with the mean aerosol optical depth (440 nm) of 0.58, 0.49, 1.18 and 1.04 for 2-, 3-I/II and 4-peak VPSD types, while the correspondingly mean relative humidity values are 58, 54, 72 and 67%, respectively. The results also show the significant increase (from 0.25 to 0.40 μm) of the mean extra peak median radius in the accumulation mode for the 3-peak-II cases, which agrees with aerosol hygroscopic growth related to relative humidity and/or cloud or fog processing.

Keywords: multi-peak aerosol volume particle size distribution, lognormal mode separation, extra fine and coarse mode peaks, hygroscopic growth

1. Introduction

Atmospheric aerosols play important roles in Earth's environment and radiation budget. The aerosols affect the climate system by scattering and absorbing solar radiation, referred to as direct effects (Stocker et al. 2013). Also, they act as cloud condensation nuclei and ice nuclei involved in cloud process, referred to as indirect effects. The increase of aerosol particles can lead to the cloud layer for rapid adjustments, precipitation reduction and longer cloud lifetime (Lohmann and Feichter 2005; Albrecht 1989; Twomey 1977). Abundant anthropogenic aerosols also cause frequent air pollution events in developing countries, e.g East of China (Li et al. 2013). Therefore, characterization of key aerosol's parameters in hot spot areas becomes important due to impacts of aerosols both on climate changes and air pollution control.

Aerosol size distribution is one of the important information of aerosol properties. The particulates suspended in the air change their sizes by coagulation, aggregation and condensation, which all vary with the aerosol size distribution. Although the particle size changes constantly, Willeke and Whitby (1975) found that atmospheric aerosol particles exist in three modes stably. The aerosol particles with diameter from 0.1μm to 1μm are referred to as accumulation mode, while those less than 0.1μm referred to as transient nuclei mode, and those more than 1μm referred to as coarse mode. Most of researches now follow this definition (e.g. Remer and Kaufman 2006; Bellouin et al. 2005; Kaufman et al. 2005a, b). The nuclei modal aerosols derived from nucleation process can be observed on the nanometer scale (e.g. Liu et al. 2013; Kulmala et al. 2004). The accumulation modal aerosols are mainly contributed by aging nuclei mode. The collision cross section of accumulation particles is about one order smaller than their geometric cross section, and thus they are hard to deposit due to viscosity of atmosphere (Park et al. 1999, Otto et al. 1999). Due to their longer residence time and important impacts on atmospheric radiation, the accumulation modal aerosols are investigated extensively.

Eck et al. (2003a, b) find that accumulation modal volume median radius of

biomass burning aerosol increases with aerosol optical depth (AOD), caused by the aerosol aging (Reid et al. 1998), and the similar phenomenon is also observed in urban-industrial and mixed site (Dubovik et al. 2002). Furthermore, two peaks in the accumulation mode can present simultaneously (i.e. Zhang et al. 2015) in the serious air pollution conditions, and the second one is considered as the residual of cloud/fog droplet evaporation (Li et al. 2014; Eck et al. 2012). The coarse modal aerosols can also present the 2-peak distribution. The first peak of coarse mode with the median radius from 1μm to 2μm is considered to result from hygroscopic growth or the activated particles with radius less than 1μm (Yang and Wenig 2009; Singh et al. 2004). As cloud condensation nuclei or ice nuclei, the first peak of the coarse mode are thought to be involved in the cloud/fog formation and dissipation (Hammer et al. 2014). All of these studies analyze the entire aerosol size distribution, rather than extract individual each characteristic peaks, except Li et al. (2014) fitted a lognormal function for extra peak of accumulation mode during heavy pollution condition.

In this study, we split the columnar aerosol volume particle size distribution retrieved by Sun-sky radiometer measurements in Beijing over 2013 into lognormal peaks based on a separation method (Cuesta et al. 2008), and analyze the recognized extra peaks with aerosol optical properties and meteorological conditions. The data and method are described in section 2. In section 3, the properties of extra peaks and ambient atmospheric conditions are analyzed, and the conclusions are provided in section 4.

2. Data and Method

2.1 Data

In this paper, the optical and physical properties of atmospheric aerosol are obtained from the Sun-sky radiometer (CE318). The CE318 has 8 channels including 340 nm, 380 nm, 440 nm, 500 nm, 675 nm, 870 nm, 1020 nm and 1640 nm for aerosol measurements, and 936 nm for perceptible water. The direct and diffused Sun light are measured from ground by CE318 and then used to derive aerosol

properties, such as AOD from extinction of incident direct sunlight, and aerosol VPSD retrieved from sky light (Dubovik et al. 2000a, b). The temporal resolutions of these two measurements are about 15 minutes and 1 hour, respectively. The Sun-sky radiometers have been applied extensively to measure atmospheric aerosol properties, as known as the AErosol RObotic NETwork (AERONET) (Holben et al. 1998, 2001).

A Sun-sky radiometer (#350) belonging to AERONET site Beijing_RADI (116.4° E, 40.0° N, 59m) is employed in this study. The AERONET Lev 1.5 data in 2013 is used including AOD, Ångström exponent (AE), single scattering albedo (SSA) and aerosol volume size distribution. The errors of AOD and SSA provided by AERONET are about 0.01-0.02 (Holben et al. 1998； Eck, et al. 1999) and 0.03 (Dubovik et al. 2000b), respectively. The AE is computed by linear regression of the 440, 500, 675, and 870 nm AOD data. The Lev 1.5 data is further filtered with additional quality controls in this paper, including (i) solar zenith angles greater than 50 degrees, (ii) the minimum number of observation angles specified by AERONET Lev 2.0 data criteria (Holben et al., 2006), and (iii) the total retrieval residual less than 5%. Moreover, the extra quality control of AOD (440 nm) > 0.4 is applied to SSA.

The meteorological data at World Meteorological Organization (WMO) Beijing site (54511, 116.5° E, 39.8° N, 31.3m) are used, including temperature, relative humidity and mean wind speed during 10 minutes, with temporal resolution of 1 hour fitting for AERONET size distribution data.

2.2 Method

In this study, we need to separate the aerosol volume particle size distribution (VPSD) into Log-Normal Modes (LNM). We employ the separation method developed by Cuesta et al. (2008). Each LNM is described by 3 parameters: the modal concentration, modal radius and geometric standard deviation. In order to obtain these parameters, a kernel function consist of root mean square differences

between VPSDs (the one calculated from combination of separated LNMs vs. the one obtained from AERONET data) is minimized, iteratively using the NelderMead simplex algorithm (Cuesta et al. 2008). The NelderMead simplex algorithm searches the convergence by applying the strictly convex function for multidimensional unconstrained minimization (Lagarias et al, 1998). We choose multi-modal lognormal distributions to fit the AERONET retrievals by the following formula:

$$\frac{dV(r)}{dlnr} = \sum_{i=1,n} \frac{C_i}{\sqrt{2\pi}(ln\sigma_i)^2} exp\left[-\frac{1}{2}\left(\frac{lnr-lnr_i}{ln\sigma_i}\right)^2\right] \quad (1)$$

where dV/dln$r$ (in unit of μm^3/μm^2) is aerosol volume particle size distribution, C_i (μm^3/μm^2), r_i (μm) and σ_i are the volume modal concentration, median radius and standard deviation of each LNM mode, respectively. Here, n is the total number of LNM modes.

The LNM separation is achieved when the second derivative of a theoretical Gaussian curve is less than zero. However, some non-significant convex functions can lead to a larger unreal total number (e.g. 6) of n (Cuesta et al. 2008). Based on data statistics and analysis of Beijing 2013 data in this paper, we find that for the purpose of identifying LNM peaks, one can use the second derivative of -0.003 as the threshold. Under this threshold, VPSD is only separated into 2 to 4 peaks, with low convergence errors. In Figure 1, we show the mode separation of an example VPSD from Beijing 2013 data.

3. Results

3.1 VPSD peak characteristics

In 2013, the number of AERONET retrieved size distribution records is 577 in Beijing site and the proportion of the available separation cases are 98.6% while the remainders are mainly non-smooth VPSDs. The recognized 2-, 3- and 4- peak type VPSD numbers account for 48%, 49% and 3% of total 569 cases (Figure 2), respectively. In figure 3, we show the statistics (N=277) on the appearance frequency of the median radii for 3-peak cases. It can be seen clearly that two distinguishable groups located in accumulation (<0.7 μm) and coarse (>0.7 μm) particle radius

ranges, respectively, which supports the classification of 3-peak-I (i.e., an extra coarse mode peak) and 3-peak-II (i.e., an extra accumulation mode peak) types in this study. Therefore, a total of four types of volume size distribution are summarized in this study and their mean VPSD are shown in Figure 2.

It can be seen from Figure 2(a) that mean volume of 3-peak-II type, especially the fine modal volume, is larger than others. The 4-peak VPSD numbers are smaller, but the mean volume is larger (Figure 2b). As listed in table 1, for accumulation mode range (i.e. r_1 and r_2), the first peak is around 0.13-0.15μm while the second peaks present at a mean median radius of 0.38 μm (±0.11) for 3-peak-II and 0.28 μm (±0.09) for 4-peak type, respectively. Moreover, two peak characteristics can also present in the coarse mode (i.e. 3-peak-I type), with the mean median radius varying from 1.25 μm (±0.56) to 1.47 μm (±0.30).

The seasonal changes of multi-peak VPSDs are also noticeable. Figure 4 shows that the 2-peak cases are prevalent in November, December and January, and the 3-peak-I prevalent in April, May. Especially in April, the 3-peak-I and II cases account for 74% of available VPSDs. In June, due to the impacts of cloud and rain on remote sensing observation, there are only 8 available VPSDs, while the summarized percentage of 3-peak-II and 4-peak cases is about 50%, the maximum in the whole year. It should also be noticed that, the VPSDs with more than 2 peaks (i.e. 3-peak and 4-peak types) appears in all months of the year. Considering that a large part of these extra peak VPSDs may related to residual of cloud/fog residuals, it is suggested that cloud contamination (e.g. thin cirrus) on the aerosols occurs (Eck et al., 2014) throughout the year in Beijing 2013.

3.2 Optical properties of multi-peak VPSDs

It is important to reveal the aerosol optical properties associated with multi-peak VPSDs. Figure 5(a) shows the frequency of multi-peak VPSD case numbers with AOD. The number frequency of the 3-peak-II and 4-peak cases increases obviously when AOD is more than 0.5. The mean AOD of the 3-peak-II

cases is the highest (1.18) in 2013 while much lower for the 3-peak-I (0.49) and 2-peak cases (0.58) as listed in Table 2. The 65% of the 2-peak cases present in the low aerosol loading conditions (e.g. AOD < 0.5), where probability of the 4-peak cases is very low (<6%).

In figure 5(b), the maximum frequency of 2- and 3-peak-I cases appear at the positions where AE equals to about 1.4, while AE is 1.3 for the 4-peak cases. For 3-peak-II cases, it presents two maximum frequencies at about AE = 1.2 and 1.4 with the frequency of 22 and 20%, respectively. This suggests there might be a sight particle size decrease effect (AE from 1.2 to 1.4) for 3-peak-II type while the more prevalent cases are with AE = 1.2. It should also be mentioned that although this standard AEORNET AE are widely used in many studies (Dubovik et al., 2002; Gobbi et al., 2007; Che et al., 2014), more information might be retrieved from AE computed from the extended wavelengths (i.e. 380-550nm) following analyses of Eck et al. (2014).

In figure 5(c), the mean SSA of 2-peak and 3-peak-I type are lower than those of 3-peak-II and 4-peak cases, suggesting that the aerosol scattering property is enhanced in 3-peak-II and 4-peak types, especially the 3-peak-II. The mean SSA at 675nm changes from 0.874 (3-peak-I) to 0.909 (3-peak-II) as listed in Table 2. Moreover, the mean SSA of 3-peak-II type is close to that of 4-peak type at 440 nm but larger at other three wavelengths. This may indicate more brown carbon and water content in aerosols for 3-peak-II type according to SSA spectral behaviors of aerosol components (Wang et al., 2013). It should be noticed that this SSA analysis may have limitations on the sample representativeness, especially for 2-peak type, considering data quality control of AOD (440 nm) > 0.4 affecting mainly on 2-peak cases. The retrieval of SSA in low AOD conditions may be improved by involving the coincident polarized measurements (Li et al. 2009) in the near future.

3.3 Relationship between VPSD peaks and meteorological factors

Figure 6 shows the number frequencies of multi-peak VPSDs with the

temperature, relative humidity, and wind speed. The mean temperature of 3-peak-I cases is about 10.8 ˚C, higher than that of the other VPSDs (see also Table 2). It is found that the maximum frequency of 3-peak-II cases occur at a lower temperature about -8 ˚C, while that of 4-peak cases is much higher (~18 ˚C). The rather random frequency distribution of 2-peak cases confirms that the 2-peak VPSDs are appeared uniformly throughout the year with varying temperature; while 3-peak-I VPSDs tend to occur during higher temperature conditions, i.e. summer and late spring. Moreover, 4-peak cases also occur mainly during summer and early spring but with slightly lower temperature than 3-peak-I type. Particularly, 3-peak-II cases often occur in the low temperature conditions, which accounts for up to 64% in winter (December, January and February).

The frequency distributions of multi-peak VPSD case numbers on relative humidity are shown in figure 6b. The 4-peak cases mainly present in the condition of relative humidity (RH) more than 40%, and the frequency peaks appear near RH of 40%-50% and 70-90%. Meanwhile, the 3-peak-II cases mainly concentrate in the RH range of 60% to 90%. The number frequencies of other two types present a roughly symmetric distribution with RH from 10% to 90%. These higher RH associated with frequency peaks can be related to aerosol hygroscopic growth (Pilinis et al. 2014; Tang and Munkelwitz 1994), and also contacted with the cloud/fog processing (Li et al. 2014).

Figure 6(c) shows that the higher number frequency of the 4-peak cases presents mainly in the condition of lower wind speed (WS < 3 m/s). Together with Figure 6(a, b), we found that 3-peak-II and 4-peak cases are mainly appear during air pollution conditions with higher aerosol loading (AOD > 0.5), lower wind speed (WS < 3m/s), and higher relative humidity (RH > 40%).

3.4 VPSD peak correlation with relative humidity

We have seen some complex relationships between multi-peak VPSDs frequency with relative humidity in Figure 6(b), whereas several researches also

suggested possible big influence of RH on extra VPSD peaks through hygroscopic effects. Here, we show a statistics on the median radius of VPSD peaks with RH bins in Table 3. It can be seen firstly a general increase of r_1 with RH, agreeing with Eck et al. (2012) results. This can be thought as the classical hygroscopic growth and/or cloud or fog processing. Secondly, r_4 show generally decreasing trends with RH, suggesting the wet scavenging effects on dust-like particles in coarse mode. Thirdly, r_2 and r_3 of 3-peak-II and 4-peak VPSDs illustrate generally a positive correlation with RH which can be thought as similar phenomena as hygroscopic growth but occurring for particles with different size (Li et al. 2014; Reid et al. 1998). The radii of aerosol particles can increase from accumulation to coarse size involved into the cloud/fog process under highly RH conditions (Klein and Dabas, 2014), while the decrease of RH results in the evaporation of cloud/fog droplets and the residual particles (Li et al., 2014) can form the extra peak around 0.25-0.40 μm (Table 3). Fourthly, r_3 of the 3-peak-I VPSD cases present a general negative correlation with RH, in contrast with those of 3-peak-II and 4-peak types. This negative correlation is thought to be associated with hydrophobic fly ash from coal combustion or other sources.

4. Conclusions

In this study, the aerosol volume particle size distributions (VPSD) retrieved from Sun-sky radiometer measurements are decomposed into characteristic log-normal peaks in Beijing over 2013. The number frequency of the 2-, 3-I/II and 4-peak cases are presented against the aerosol optical properties and meteorological conditions. It is found that the most part of VPSDs present two characteristic peaks, while the probability of double-peak pattern in a single mode (accumulation and/or coarse modes) increases under pollution conditions. The extra fine and coarse modal peaks are identified in this study with the mean center radius of about 0.28(±0.09)-0.38(±0.11) and 1.25(±0.56)-1.47(±0.30) μm, respectively, in contrast with those of standard peaks (0.15 and 3.71 μm). The 3-peak-I type appears under

dry conditions (mean RH of 54%) and is thought to contain hydrophobic fly ash particles. The 3-peak-II and 4-peak types prevalently present in the condition of large aerosol loading and high humidity (mean RH of 72% and 67%, respectively) conditions, with the mean AOD (440 nm) of 1.18 and 1.04, and mean SSA (675 nm) of 0.909 and 0.902, respectively. The correlations between multi-peak VPSD appearance and RH suggest that the aerosol hygroscopic/hydrophobic changes and cloud/fog process can play important roles in the aerosol size transformation.

We also noticed that in Beijing the extra coarse peaks (mean median radii around 1.25 and 1.47 μm) possibly associate with two different sources/mechanisms, considering their opposite RH dependence. The aerosol components are not analyzed in this study, considering component information from in situ measurements is somehow difficult to match exactly remote sensing measurement (i.e. surface quantities vs. total column values). In the future, with the development of aerosol component inversion techniques based on remote sensing data (e.g. Schuster et al. 2015), coupling with the characteristic peak analyses, it is expected to estimate aerosol component information inside each characteristic peaks, which helps understand particulate formation and transformation in the ambient atmosphere.

Acknowledgement

This work was supported by National Natural Science Fund of China (No. 41222007), the Chinese Academy of Sciences Key Deployment project (No. KZZD-EW-TZ-18), the CAS Strategic Priority Research Program (no. XDA05100202), and the Chinese Major Project of High Resolution Earth Observation System (30-Y20A39-9003-15/17).

References

Albrecht B (1989) Aerosols, cloud microphysics and fractional cloudiness. Science 245: 1227–1230.

Bellouin N, Boucher O, Haywood J, and Reddy MS (2005) Global estimate of

aerosol direct radiative forcing from satellite measurements. Nature 438: 1138-1141.

Che H, Xia X, and Zhu J et al (2014) Aerosol optical properties under the condition of heavy haze over an urban site of Beijing, China. Environ Sci Pollut Res DOI 10.1007/s11356-014-3415-5.

Cuesta J, Flamant PH, and Flamant C (2008) Synergetic technique combining elastic backscatter lidar data and sunphotometer AERONET inversion for retrieval by layer of aerosol optical and microphysical properties. Appl Optics 47: 4598-4611.

Dubovik O, Holben B, Eck TF, Smirnov A, Kaufman YJ, King MD, Tanre D, and Slutsker I (2002) Variability of absorption and optical properties of key aerosol types observed in worldwide locations. J Atmos Sci 59: 590-608.

Dubovik O and King MD (2000a) A flexible inversion algorithm for retrieval of aerosol optical properties from Sun and sky radiance measurements. J Geophys Res-Atmos 105: 20673-20696.

Dubovik O, Smirnov A, Holben BN, King MD, Kaufman YJ, Eck TF, and Slutsker I (2000b) Accuracy assessments of aerosol optical properties retrieved from Aerosol Robotic Network (AERONET) Sun and sky radiance measurements. J Geophys Res-Atmos 105: 9791-9806.

Eck TF, Holben BN, and Reid JS et al (2014) Observations of rapid aerosol optical depth enhancements in the vicinity of polluted cumulus clouds. Atmos. Chem. Phys. 14: 11633-11656.

Eck TF, Holben BN, Reid JS et al. (2012) Fog- and cloud-induced aerosol modification observed by the Aerosol Robotic Network (AERONET). J Geophys Res-Atmos 117: D07206, doi:10.1029/2011JD016839.

Eck TF, Holben BN, Reid JS, O'Neill NT, Schafer JS, Dubovik O, Smirnov A, Yamasoe MA, and Artaxo P (2003a) High aerosol optical depth biomass burning events: A comparison of optical properties for different source regions.

Geophys Res Lett. doi:10.1029/2003GL017861.

Eck TF, Holben BN, Ward DE, Mukelabai MM, Dubovik O, Smirnov A, Schafer JS, Hsu NC, Piketh SJ, Queface A, Le Roux J, Swap RJ, and Slutsker I (2003b) Variability of biomass burning aerosol optical characteristics in southern Africa during the SAFARI 2000 dry season campaign and a comparison of single scattering albedo estimates from radiometric measurements. J Geophys Res-Atmos. doi: 10.1029/2002JD002321.

Eck TF, Holben BN, Reid JS, Dubovik O, Smirnov A, O'Neill NT, Slutsker I, and Kinne S (1999) Wavelength dependence of the optical depth of biomass burning, urban, and desert dust aerosols. J Geophys Res-Atmos 104: 31333-31349.

Gobbi GP, Kaufman YJ, Koren I & Eck TF (2007) Classification of aerosol properties derived from AERONET direct sun data. Atmospheric Chemistry and Physics 7: 453-458.

Hammer E, Gysel M, Roberts GC, Elias T, Hofer J, Hoyle CR, Bukowiecki N, Dupont JC, Burnet F, Baltensperger U, and Weingartner E (2014) Size-dependent particle activation properties in fog during the Paris Fog 2012/13 field campaign. Atmos Chem Phys 14: 10517-10533.

Holben, BN, Eck TF, Slutsker I, Smirnov A, Sinyuk A, Schafer J, Giles D, and Dubovik O (2006) AERONET's version 2.0 quality assurance criteria Remote Sensing of Atmosphere and Clouds. Proc SPIE Int Soc Opt Eng 6408: 64080Q doi:10.1117/12.706524.

Holben BN, Tanre D, Smirnov A, Eck TF, Slutsker I, Abuhassan N, Newcomb WW, Schafer JS, Chatenet B, Lavenu F, Kaufman YJ, Castle JV, Setzer A, Markham B, Clark D, Frouin R, Halthore R, Karneli A, O'Neill NT, Pietras C, Pinker RT, Voss K, and Zibordi G (2001) An emerging ground-based aerosol climatology: Aerosol optical depth from AERONET. J Geophys Res-Atmos 106: 12067-12097.

Holben BN, Eck TF, Slutsker I, Tanre D, Buis JP, Setzer A, Vermote E, Reagan JA,

Kaufman YJ, Nakajima T, Lavenu F, Jankowiak I, and Smirnov A (1998) AERONET - A federated instrument network and data archive for aerosol characterization. Remote Sens Environ 66: 1-16.

Kaufman YJ, Boucher O, Tanre D, Chin M, Remer LA, and Takemura T (2005a) Aerosol anthropogenic component estimated from satellite data. Geophys Res Lett. doi: 10.1029/2005GL023125.

Kaufman YJ, Koren I, Remer LA, Tanre D, Ginoux P, and Fan S (2005b) Dust transport and deposition observed from the Terra-Moderate Resolution Imaging Spectroradiometer (MODIS) spacecraft over the Atlantic ocean. J Geophys Res-Atmos. doi: 10.1029/2003JD004436.

Klein C and Dabas A (2014) Relationship between optical extinction and liquid water content in fogs. Atmos Meas Tech 7: 1277-1287.

Kulmala M, Vehkamaki H, Petaja T, Dal Maso M, Lauri A, Kerminen VM, Birmili W, and McMurry PH (2004) Formation and growth rates of ultrafine atmospheric particles: a review of observations. J Aerosol Sci 35: 143-176.

Lagarias JC, Reeds JA, Wright MH, and Wright PE (1998) Convergence properties of the Nelder-Mead simplex method in low dimensions. Siam J Optim 9(1):112-147.

Li Z, Eck T, Zhang Y, Zhang Y, Li D, Li L, Xu H, Hou W, Lv Y, Goloub P, and Gu X (2014) Observations of residual submicron fine aerosol particles related to cloud and fog processing during a major pollution event in Beijing. Atmos Environ 86: 187-192.

Li Z, Gu X, Wang L, Li D, Xie Y, Li K, Dubovik O, Schuster G, Goloub P, Zhang Y, Li L, Ma Y, and Xu H (2013) Aerosol physical and chemical properties retrieved from ground-based remote sensing measurements during heavy haze days in Beijing winter. Atmos Chem Phys 13: 10171-10183.

Li Z, Goloub P., Dubovik O., Blarel L., Zhang W., Podvin T., Sinyuk A., Sorokin M., Chen H., Holben B., Tanre D., Canini M., Buis J.P. (2009) Improvements for

ground-based remote sensing of atmospheric aerosol properties by additional polarimetric measurements. Journal of Quantitative Spectroscopy & Radiative Transfer 110: 1954-1961.

Liu X, Li J, Qu Y, Han T, Hou L, Gu J, Chen C, Yang Y, Liu X, Yang T, Zhang Y, Tian H, and Hu M (2013) Formation and evolution mechanism of regional haze: a case study in the megacity Beijing, China. Atmos Chem Phys 13: 4501-4514.

Lohmann U, and Feichter J (2005) Global indirect aerosol effects: Areview. Atmos Chem Phys 5: 715–737.

Otto E, Fissan H, Park SH, and Lee KW (1999) The log-normal size distribution theory of Brownian aerosol coagulation for the entire particle size range: Part II - Analytical solution using Dahneke's coagulation kernel. J Aerosol Sci 30: 17-34.

Park SH, Lee KW, Otto E, and Fissan H (1999) The log-normal size distribution theory of Brownian aerosol coagulation for the entire particle size range: Part I - Analytical solution using the harmonic mean coagulation kernel. J Aerosol Sci 30: 3-16,.

Pilinis C, Charalampidis PE, Mihalopoulos N, and Pandis SN (2014) Contribution of particulate water to the measured aerosol optical properties of aged aerosol. Atmos Environ 82: 144-153.

Reid JS, Hobbs PV, Ferek RJ, Blake DR, Martins JV, Dunlap MR, and Liousse C (1998) Physical, chemical, and optical properties of regional hazes dominated by smoke in Brazil. J Geophys Res-Atmos 103: 32059-32080.

Remer LA and Kaufman YJ (2006) Aerosol direct radiative effect at the top of the atmosphere over cloud free ocean derived from four years of MODIS data. Atmos Chem Phys 6: 237-253.

Singh RP, Dey S, Tripathi SN, Tare V, and Holben B (2004) Variability of aerosol parameters over Kanpur, northern India. J Geophys Res-Atmos. doi: 10.1029/2004JD004966.

Schuster GL, Dubovik O, and Arola A (2015) Remote sensing of soot carbon – Part 1: Distinguishing different absorbing aerosol species. Atmos Chem Phys Discuss 15: 13607-13656.

Stocker TF, Qin D, Plattner GK, Tignor M, Allen SK, Boschung J, Nauels A, Xia Y, Bex V and Midgley PM (2013) Climate Change 2013: The Physical Science Basis. Contribution of Working Group I to the Fifth Assessment Report of the Intergovernmental Panel on Climate Change. Cambridge University Press Cambridge, United Kingdom and New York.

Tang IN and Munkelwitz HR (1994) Water Activities, Densities, and Refractive-Indexes of Aqueous Sulfates and Sodium-Nitrate Droplets of Atmospheric Importance, J Geophys Res-Atmos 99: 18801-18808.

Twomey S (1977) Influence of Pollution on Shortwave Albedo of Clouds. J Atmos Sci 34: 1149-1152.

Willeke K and Whitby KT (1975) Atmospheric Aerosols: Size Distribution Interpretation. J Air Pollut Contr Assoc 25(5): 529-534.

Wang L, Li Z, Tian Q, Ma Y, Zhang F, Zhang Y, Li D, Li K, and Li L (2013) Estimate of aerosol absorbing components of black carbon, brown carbon, and dust from ground-based remote sensing data of sun-sky radiometers. 118: 1-10 doi: 10.1002/jgrd.50356.

Yang X and Wenig M (2009) Study of columnar aerosol size distribution in Hong Kong. Atmos Chem Phys 9: 6175-6189.

Zhang Y, Li Z, Cuesta J, Li D, Wei P, Xie Y, and Li L (2015) Aerosol Column Size Distribution and Water Uptake Observed during a Major Haze Outbreak over Beijing on January 2013. Aerosol Air Qual Res 15: 945–957.

List of Table Captions

Table 1. Three log-normal mode parameters (r, σ, C) of VPSD of Figure 2.

Table 2. The optical, physical and meteorological parameters corresponding to VPSD types with multiple peaks.

Table 3. The mean median radius of multi-peak VPSD types under different relative humidity (RH) bins.

List of Figure Captions

Figure 1. Aerosol volume particle size distribution and the corresponding sepration into four log-normal modes.

Figure 2. The annual mean VPSD of 2-peak, 3-peak-I, 3-peak-II cases (a); and 4-peak cases (b) in Beijing 2013.

Figure 3. The number frequency of median radius for the extra peaks of 3-peak VPSDs.

Figure 4. The monthly percentage of multi-peak VPSDs in Beijing 2013.

Figure 5. The number frequency of multi-peak VPSDs versus AOD (a), AE (b) and SSA (c). AOD: aerosol optical depth; AE: Ångström exponent; SSA: single scattering albedo; the x-axis step is 0.1 in (a) and (b).

Figure 6. The number frequency of multi-peak VPSDs versus temperature (5˚C interval) (a), relative humidity (5% interval) (b) and wind speed at altitude of 10 m (0.5 m/s interval) (c).

Table 1. Three log-normal mode parameters (r, σ, C) of VPSD of Figure 2.

VPSD type	N	median radius (μm) (st.d.)				standard deviation (st.d.)				modal concentration ($\mu m^3/\mu m^2$) (st.d.)			
		r_1	r_2	r_3	r_4	σ_1	σ_2	σ_3	σ_4	C_1	C_2	C_3	C_4
2-peak	274	0.15 (0.03)	/	/	3.71 (0.93)	1.49 (0.10)	/	/	1.64 (0.16)	0.053 (0.059)	/	/	0.073 (0.073)
3-peak-I	203	0.15 (0.03)	/	1.47 (0.30)	4.20 (0.62)	1.49 (0.09)	/	2.13 (0.39)	1.54 (0.18)	0.045 (0.040)	/	0.047 (0.035)	0.069 (0.083)
3-peak-II	74	0.15 (0.05)	0.38 (0.11)	/	2.70 (0.51)	1.51 (0.26)	1.72 (0.32)	/	1.90 (0.22)	0.080 (0.049)	0.065 (0.061)	/	0.122 (0.090)
4-peak	18	0.13 (0.03)	0.28 (0.09)	1.25 (0.56)	3.44 (0.97)	1.44 (0.19)	1.57 (0.16)	1.70 (0.64)	1.72 (0.22)	0.054 (0.042)	0.064 (0.044)	0.040 (0.037)	0.088 (0.040)

Table 2. The optical, physical and meteorological parameters corresponding to VPSD types with multiple peaks.

VPSD Type	AOD (440nm)	AE	SSA (675nm)	T (℃)	RH (%)	WS (m/s)
2-peak	0.58	1.28	0.885	5.0	58	1.62
3-peak-I	0.49	1.12	0.874	10.8	54	1.88
3-peak-II	1.18	1.18	0.909	5.2	72	1.31
4-peak	1.04	1.20	0.902	6.6	66	1.58

Note: AOD: Aerosol Optical Depth; AE: Ångström Exponent; SSA: Single Scattering Albedo; T: Temperature; RH: Relative Humidity; WS: Wind Speed.

Table 3. The number frequency of median radius for the extra peaks of 3-peak VPSDs.

RH (%)		mean median radius (st.d.) [unit: μm]			
		r_1 (μm)	r_2 (μm)	r_3 (μm)	r_4 (μm)
2-peak	[0,35]	0.14 (0.018)	/	/	4.16 (0.353)
	(35,50]	0.13 (0.019)	/	/	3.76 (0.652)
	(50,70]	0.14 (0.033)	/	/	3.68 (1.381)
	(70,90]	0.16 (0.034)	/	/	3.42 (0.744)
3-peak-I	[0,35]	0.13 (0.014)	/	1.46 (0.200)	4.52 (0.557)
	(35,50]	0.14 (0.021)	/	1.57 (0.248)	4.30 (0.566)
	(50,70]	0.15 (0.024)	/	1.43 (0.347)	4.06 (0.512)
	(70,90]	0.15 (0.035)	/	1.41 (0.339)	3.89 (0.661)
3-peak-II	[0,35]	0.11 (0.012)	0.25 (0.047)	/	2.28 (0.118)
	(35,50]	0.11 (0.021)	0.32 (0.123)	/	2.57 (0.368)
	(50,70]	0.13 (0.048)	0.40 (0.125)	/	2.85 (0.521)
	(70,90]	0.18 (0.049)	0.40 (0.106)	/	2.65 (0.521)
4-peak	[0,35]	/	/	/	/
	(35,50]	0.13 (0.034)	0.29 (0.084)	1.27 (0.497)	3.83 (1.219)
	(50,70]	0.11 (0.025)	0.21 (0.044)	1.00 (0.277)	3.45 (0.871)
	(70,90]	0.13 (0.030)	0.30 (0.096)	1.18 (0.553)	3.06 (0.806)

Figure 1

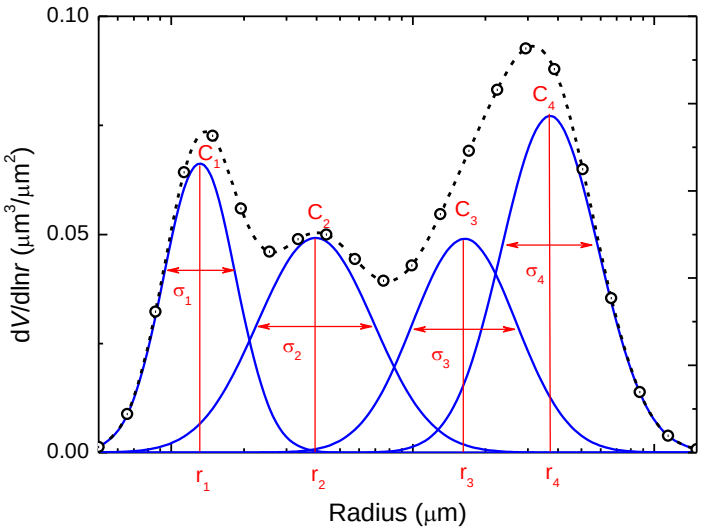

Figure 1. Aerosol volume particle size distribution and the corresponding separation into four log-normal modes.

Figure 2

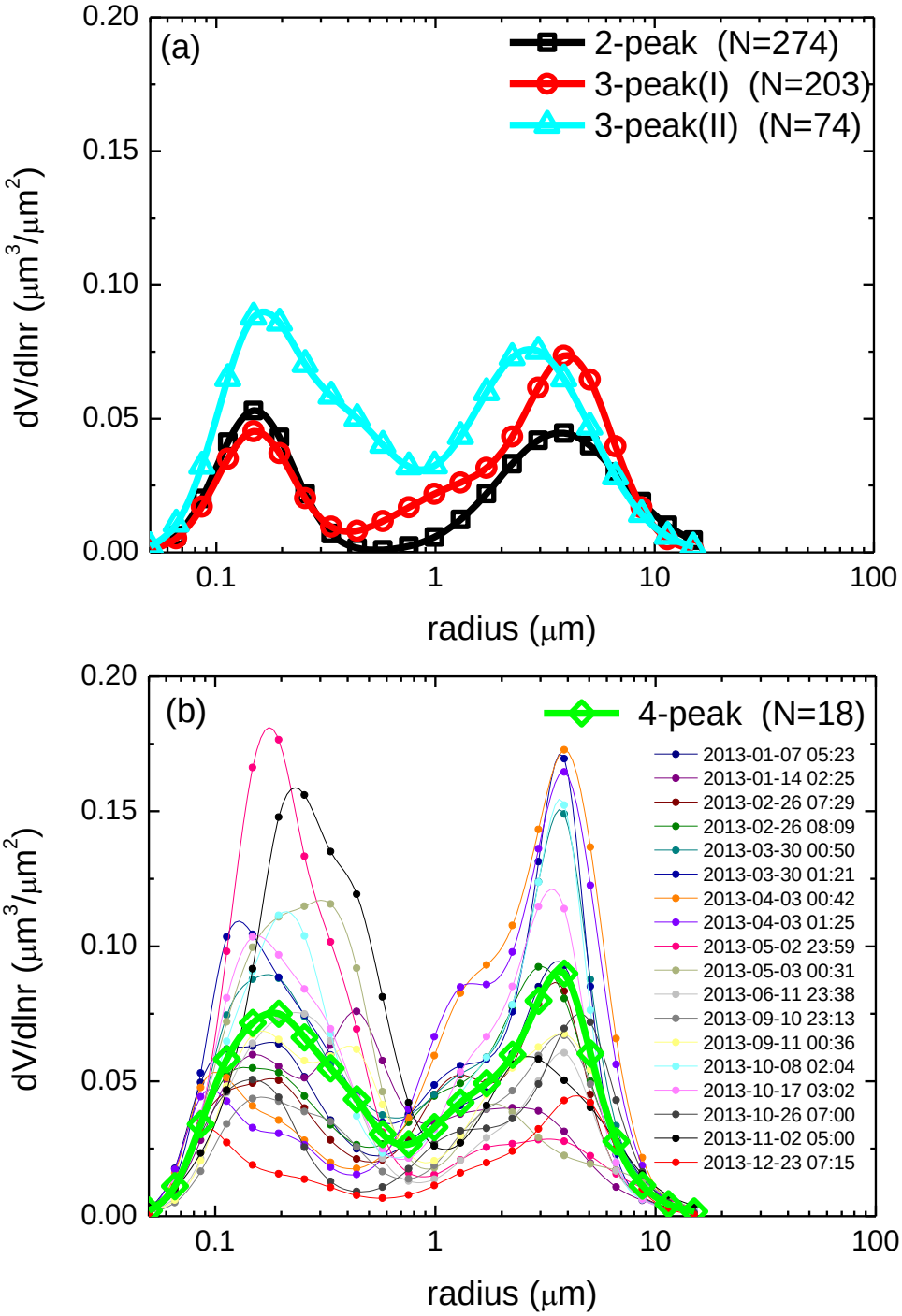

Figure 2. The annual mean VPSD of 2-peak, 3-peak-I, 3-peak-II cases (a); and 4-peak cases (b) in Beijing 2013.

Figure 3

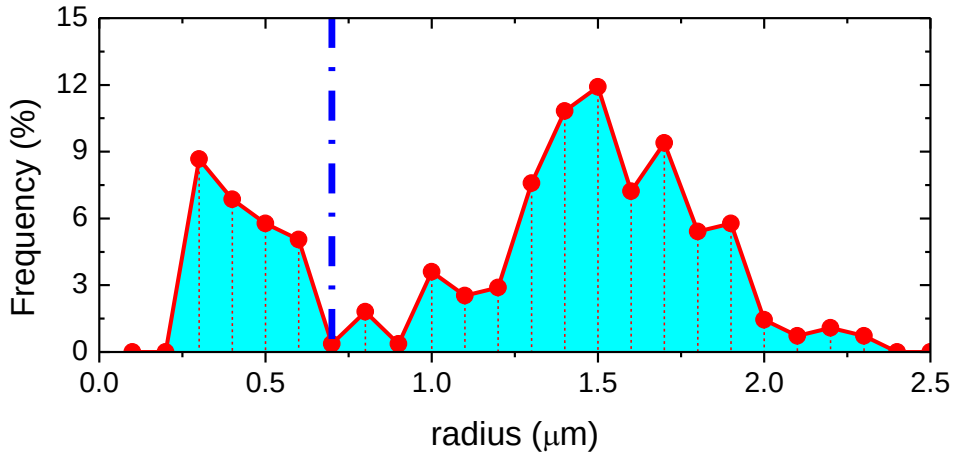

Figure 3. The number frequency of median radius for the extra peaks of 3-peak VPSDs.

Figure 4

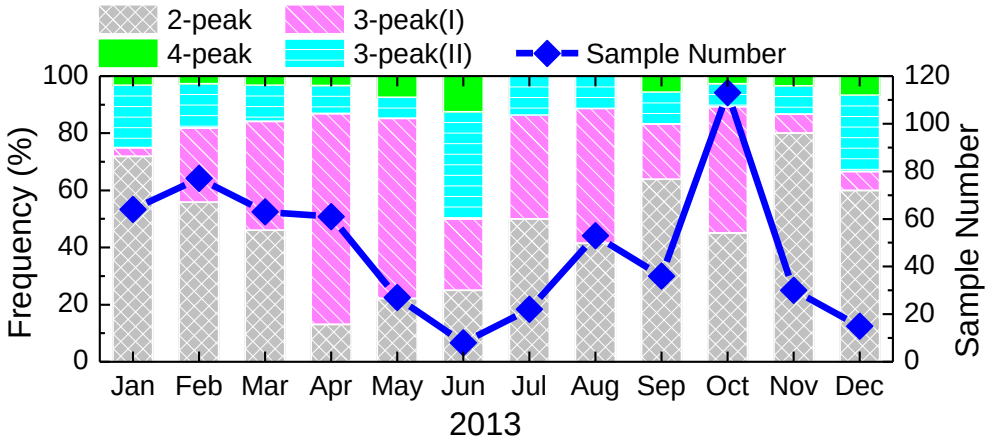

Figure 4. The monthly percentage of multi-peak VPSDs in Beijing 2013.

Figure 5

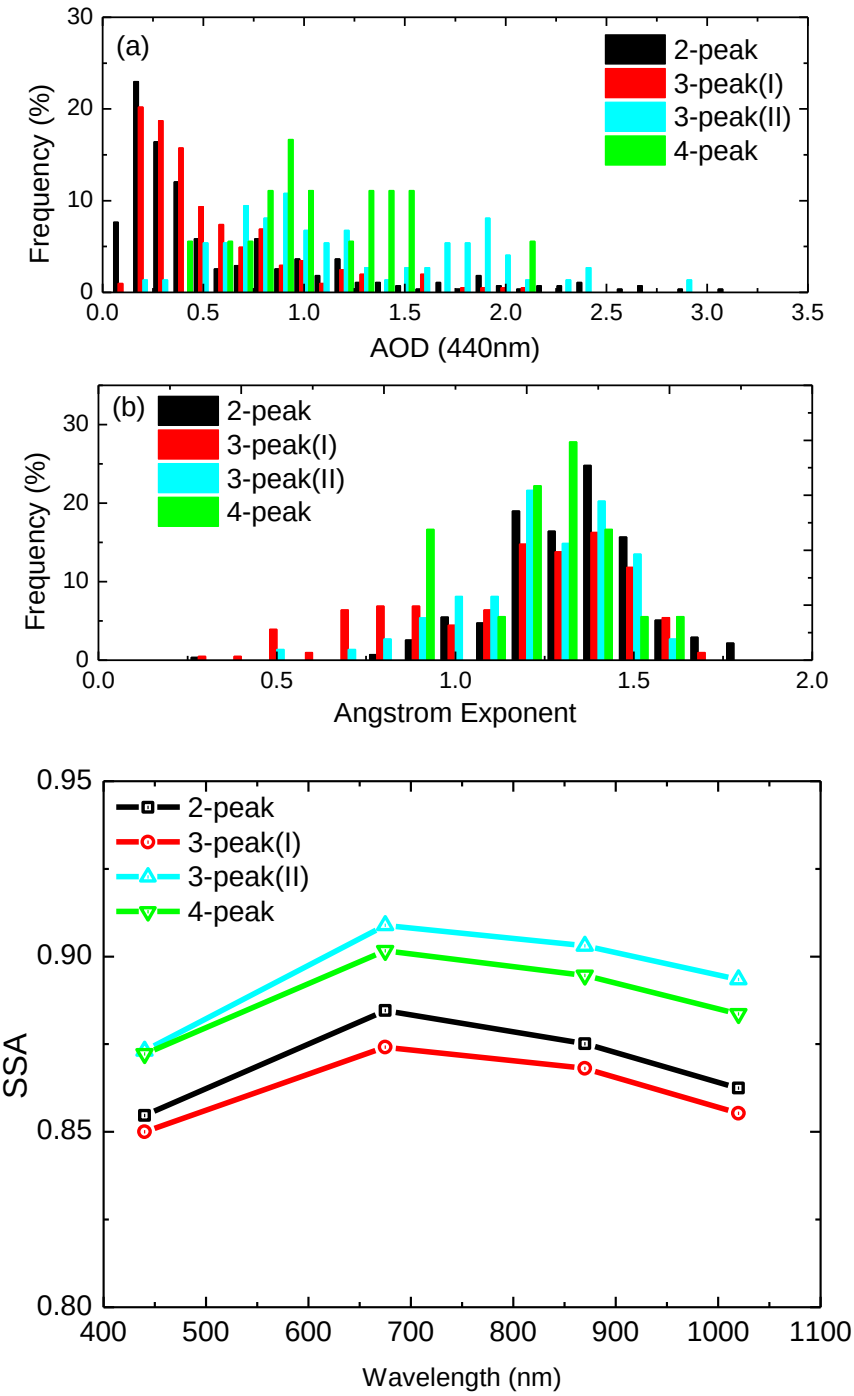

Figure 5. The number frequency of multi-peak VPSDs versus AOD (a), AE (b) and SSA (c). AOD: aerosol optical depth; AE: Ångström exponent; SSA: single scattering albedo; the x-axis step is 0.1 in (a) and (b).

Figure 6

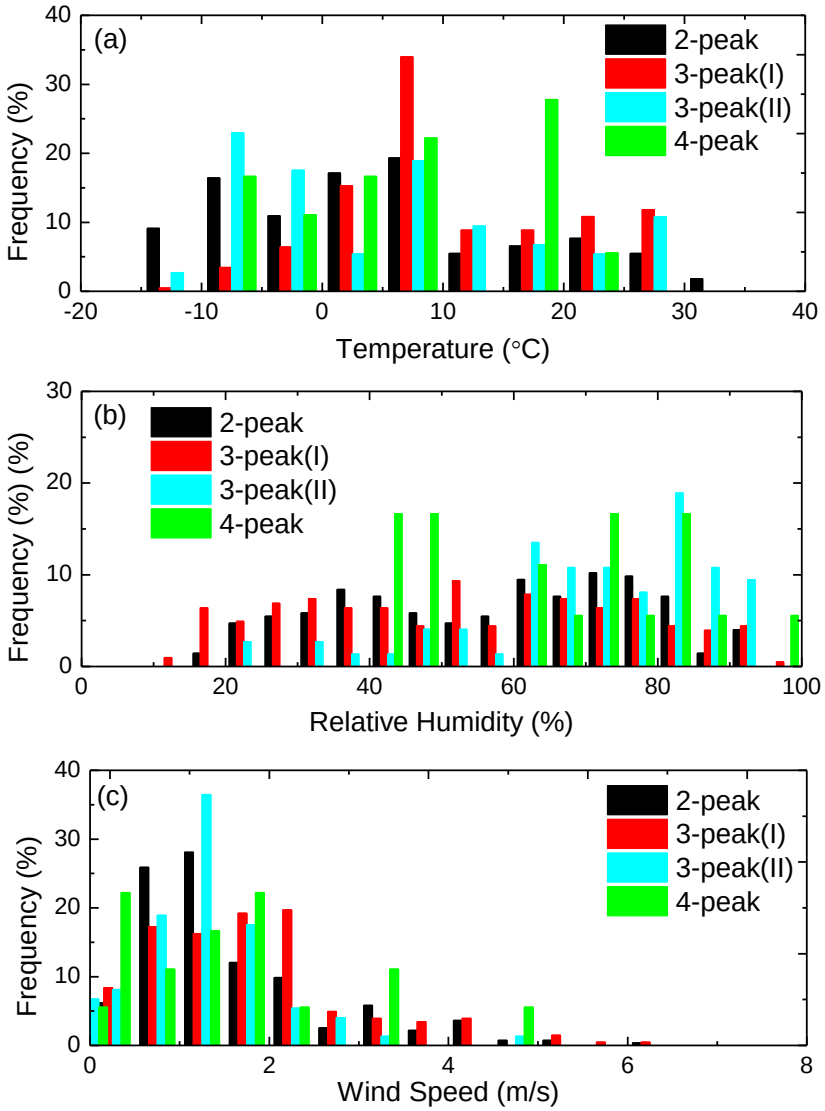

Figure 6. The number frequency of multi-peak VPSDs versus temperature (5˚C interval) (a), relative humidity (5% interval) (b) and wind speed at altitude of 10 m (0.5 m/s interval) (c).